AIAA 2001-3872

Asymptotic Formulation of the Mean Temperature in a Solid Rocket Motor

A. B. Vyas and J. Majdalani
Marquette University
Milwaukee, WI 53233

G. A. Flandro
University of Tennessee Space Institute
Tullahoma, TN 37388

37th AIAA/ASME/SAE/ASEE Joint Propulsion Conference and Exhibit
8–11 July 2001, Salt Lake City, UT

Asymptotic Formulation of the Mean Temperature in a Solid Rocket Motor

Anand B. Vyas* and Joseph Majdalani†
Marquette University, Milwaukee, WI 53233
and
Gary A. Flandro‡
University of Tennessee Space Institute, Tullahoma, TN 37388

A preliminary investigation is undertaken to estimate the magnitudes of fundamental transport properties associated with the internal thermoacoustic field of a solid rocket motor. In light of the estimated magnitudes, the energy equation is simplified. The possibility of circumventing chemical reactions while retaining the essential physics of the problem is explored. This is accomplished by introducing a distributed heat source above the propellant surface that is equivalent to the heat released by chemical reactions. The resulting energy equation is solved to zeroth order and the solution to the next order is outlined. The analytical solution and corresponding temperature maps are found to be in agreement with numerical simulations of the combustion chamber. Specific areas that require further exploration are identified in the hope of obtaining a refined model.

Nomenclature

b = radial location of the heat source, dimensionless
c_p = specific heat at constant pressure, J/kg-K
Ec = dimensionless parameter
k = thermal conductivity, W/m-K
L = length of the motor, m
p^* = dimensional pressure, Pa
Pe = Peclet number
Pr = Prandtl number
$\dot{Q}$ = normalized heat generation per unit volume
r = dimensional radial coordinate, m
R = instantaneous inner radius of the motor, m
Re = injection Reynolds number
T^* = dimensional temperature, K
T = normalized temperature
$\hat{T}$ = normalized temperature at the throat
u^* = velocity (u_r^*, u_z^*), m/s
V = injection velocity at radius R, m/s
z^* = axial coordinate, m
z = normalized axial coordinate, z^*/L
γ = ratio of specific heats
η = transformed radial coordinate, r^*/a
μ = dynamic viscosity, kg/m-s
ρ = density, kg/m^3
ϕ = ratio of radius to length of the motor

Superscripts
* = denotes a dimensional variable

Subscripts
0 = reference value
ct = condition corresponding to the choked throat
r = radial component
s = stagnation temperature at head end
w = at the wall
z = axial component or partial derivative

*Graduate Student and Research Associate. Member AIAA.
†Assistant Professor, Department of Mechanical and Industrial Engineering. Member AIAA.
‡Boling Chair Professor of Mechanical and Aerospace Engineering. Associate Fellow, AIAA.

I. Introduction

THEORETICAL efforts geared towards understanding aeroacoustic instabilities in solid rocket motors have spanned four decades. Despite important findings realized by several investigators, the complete understanding of internal gas dynamics and related instabilities has not been fully realized. This is due to the multifaceted and interrelated nature of the phenomena involved.[1] In fact, past efforts to understand internal flow instabilities may be naively grouped into two categories: (i) those attempting to analyze the

details of unsteady combustion without giving due attention to the internal flow details;[2-7] and (ii) those attempting to elucidate the flow details while ignoring the role of unsteady combustion.[8-14]

Exceptions to these classifications exist and can be illustrated in the computational studies of Apte and Yang,[15] Roh, Tseng and Yang,[16] Roh and Culick,[17] and Vuillot and co-workers.[18,19] By focusing on numerical simulations, as opposed to analytical solutions of the internal flowfield, these thorough investigators have been partly successful in combining the complex aeroacoustic interactions with the elements of combustion. Aside from these numerical studies, the intrinsic coupling between thermal and aeroacoustic modes has been largely neglected.

In the current study, we attempt to develop a mathematical model that can couple the gas dynamics with the intense heat generated from propellant combustion. The resulting model is expected to allow for a thermally sensitive solution of the flowfield that incorporates the effects of chemical reactions and entropy gradients. At present, the effort will be to evaluate the basic temperature gradients that can mimic those generated from propellant combustion. These gradients need to be later accounted for in the complete flow formulation.

At first, the basic nature of the equations will be examined. This will enable us to identify small parameters that can be effectively used to simplify the model. The work is directed towards normalizing the energy equation by introducing a distributed heat source to replace the flame zone above the propellant surface. We also ignore, at this stage, nonlinear heat radiation. A principal task consists of providing accurate estimates for important transport properties using modern correlations. To make headway, we thus introduce essential simplifications based on empirical data. Next, we solve these equations using asymptotic expansions to the leading order and compare our results with predictions made by other researchers.

II. Mathematical Model

As shown in Fig. 1, the coordinate system is so chosen that the longitudinal axis of the motor corresponds to the z-axis. Due to an assumed symmetry about this axis, the domain of interest is reduced to $0 \le r^* \le R$, $0 \le z^* \le L$. As usual, the internal radius of the cylindrical grain is denoted by R while the length of the grain is labeled L. The case of regressing walls has been analyzed in the companion paper by Majdalani, Vyas and Flandro.[20] Nonetheless, a time-dependent radius will not be considered here for the sake of simplicity. Note that a constant heat flux is imposed along the lateral wall in a manner to account

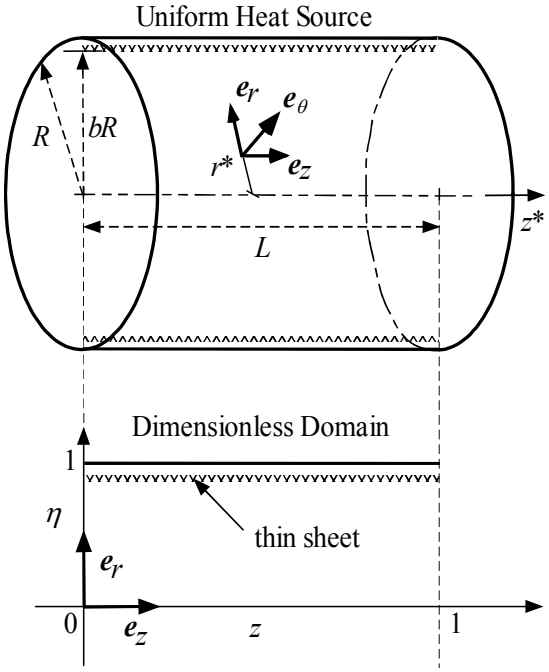

Fig. 1. Idealized motor chamber and system of coordinates illustrating the thin sheet approximation of the heat source.

for the chemical reaction energy released during surface combustion.

Without rewriting the entire set of Navier-Stokes equations, we shall first consider the energy equation during steady state conditions. We shall then normalize the result and compare its constitutive terms based on their orders of magnitude. This will enable us to recognize small quantities that can be ignored at first approximation. In fact, this will enable us to decouple, at leading order, the energy equation from the momentum equations.

A. Basic Assumptions

Following classic idealizations, the energy equation is written under the implicit assumptions that:

- The bulk flow is incompressible and steady.
- Body forces and turbulence effects are absent.
- Transport properties are constant.
- The fluid enters the tube at a uniform velocity V.
- Azimuthal variations in pressure, temperature or velocity are negligible.
- Chemical reactions are confined to a thin sheet at the burning surface.
- The flame can be replaced by a heat source.
- Heat transport by radiation inside the motor can been ignored for simplicity.

Further assumptions will be later introduced whenever necessary.

B. Governing Equation and Boundary Conditions

The energy equation under the stated assumptions can be expressed by

$$\rho c_p\left(u_r^*\frac{\partial T^*}{\partial r^*}+u_z^*\frac{\partial T^*}{\partial z^*}\right)-\left(u_r^*\frac{\partial p^*}{\partial r^*}+u_z^*\frac{\partial p^*}{\partial z^*}\right)$$
$$=\frac{k}{r^*}\frac{\partial}{\partial r^*}\left(r^*\frac{\partial T^*}{\partial r^*}\right)+k\frac{\partial^2 T^*}{\partial z^{*2}}$$
$$+\dot{Q}^*+2\mu\left[\frac{u_r^{*2}}{r^{*2}}+\left(\frac{\partial u_r^*}{\partial r^*}\right)^2+\left(\frac{\partial u_z^*}{\partial z^*}\right)^2+\tfrac{1}{2}\left(\frac{\partial \tilde{u}_z}{\partial r}\right)^2\right] \quad (1)$$

The temperature boundary conditions used in our physical setting correspond to

$$r^*=0,\ \frac{\partial T^*}{\partial r^*}=0\ ,\ r^*=R,\ T^*=T_{\rm w} \quad (2)$$

$$z^*=0,\ T^*=T_{\rm s}\ ,\ z^*=L,\ T^*=T_{\rm ct} \quad (3)$$

where $T_{\rm w}$ is the adiabatic flame temperature at the wall, $T_{\rm s}$ is the stagnation temperature at the head end, and $T_{\rm ct}$ refers to the throat condition at the downstream end.

At this stage, it is expedient to normalize Eqs. (1)–(3) using the following definitions:

$$\eta\equiv\frac{r^*}{R};\ z\equiv\frac{z^*}{L};\ u_r\equiv\frac{u_r^*}{V};\ u_z\equiv\frac{u_z^*}{V};\ p\equiv\frac{p^*}{\rho V^2} \quad (4)$$

$$\dot{Q}\equiv\frac{\dot{Q}^*}{\rho c_p\left(T_{\rm s}-T_{\rm w}\right)}\frac{R}{V}\ ;\ \text{and}\ T\equiv\frac{T^*-T_{\rm w}}{T_{\rm s}-T_{\rm w}} \quad (5)$$

Following backward substitution, the energy equation reduces to

$$u_r\frac{\partial T}{\partial\eta}+\phi u_z\frac{\partial T}{\partial z}-{\rm Ec}\left(u_r\frac{\partial p}{\partial\eta}+\phi u_z\frac{\partial p}{\partial z}\right)$$
$$=\frac{1}{\rm Pe}\left[\frac{1}{\eta}\frac{\partial}{\partial\eta}\left(\eta\frac{\partial T}{\partial\eta}\right)+\phi^2\frac{\partial^2 T}{\partial z^2}\right]+\dot{Q}$$
$$+\frac{\rm Ec}{\rm Re}\left\{2\left[\frac{u_r^{\ 2}}{\eta^2}+\left(\frac{\partial u_r}{\partial\eta}\right)^2+\left(\frac{\partial u_z}{\partial z}\right)^2\right]+\left(\frac{\partial u_z}{\partial\eta}\right)^2\right\} \quad (6)$$

where $\phi=R/L$ is the motor's aspect ratio and ${\rm Re}$, ${\rm Pr}$, ${\rm Pe}$, and ${\rm Ec}$ symbolize the Reynolds, Prandtl, Peclet, and Eckert numbers. These are given by

$${\rm Re}=\frac{VR}{\nu};\ {\rm Pr}=\frac{\mu c_p}{k};\ {\rm Pe}={\rm Re}\,{\rm Pr};\ \ {\rm Ec}=\frac{V^2}{c_p(T_{\rm s}-T_{\rm w})} \quad (7)$$

Boundary conditions in normalized form become

$$T(1,z)=0;\ \frac{\partial T(0,z)}{\partial\eta}=0;\ T(\eta,0)=1;\ T(\eta,1)=\hat{T} \quad (8)$$

where

$$\hat{T}=\frac{T_{\rm ct}-T_{\rm w}}{T_{\rm s}-T_{\rm w}}\ ;\ T_{\rm s}=\tfrac{1}{2}T_{\rm ct}\left(\gamma+1\right);\gamma=1.4 \quad (9)$$

The last relation is due to the fundamental dependence of the static temperature on the stagnation temperature for choked conditions at the downstream end. It can be developed from $T_{\rm s}=T\left[1+\frac{1}{2}(\gamma-1)M^2\right]$ for $M=1$.

C. Estimation of Transport Properties

Before proceeding further, we find it necessary to evaluate the transport properties and related parameters that appear in Eq. (6). We first start by determining the average viscosity and thermal conductivity for a gas mixture using modern empirical or semi-empirical correlations.[21]

To approximate the viscosity for a mixture of gases at high pressures and temperatures, we find the models of Lucas[22] and Chung[21] to be quite resourceful. The correlations due to Lucas necessitate the temperature, pressure, and composition as input variables while Chung's relations only require the temperature, density, and composition. As we prefer to work with pressure, temperature, velocity, and mixture composition, we opt for the Lucas expressions over Chung's. The mixture composition is utilized as suggested by Lengellé.[23] On that account, the dynamic viscosity for a gas mixture at $1000-3500\,{\rm K}$ and 10-100 bar is calculated to be approximately $10^{-5}-10^{-4}$ N-s/m^2 $(100-1000\ \mu{\rm P})$. The reader is cautioned that the routinely used formula by Sutherland,[24] namely,

$$\frac{\mu^*}{\mu_0}\approx\left(\frac{T^*}{T_0}\right)^{\frac{3}{2}}\frac{T_0+110\,{\rm K}}{T^*+110\,{\rm K}} \quad (10)$$

underestimates the viscosity by omitting pressure effects. Nonetheless, Sutherland's law can be used in the asymptotic analysis due to its simplicity, especially when compared to those obtained by Lucas or Chung. It must be noted that the latter are quite accurate and deviate from experimental observations by a maximum of 9 percent. In the companion article by Majdalani, Vyas and Flandro,[20] key parameters including the injection Reynolds number are calculated based, in part, on this data.

D. Dynamic Similarity Parameters

Using Chung's method, the thermal conductivity is found to be ≈ 2.0 W/m-K. This is roughly equal to the thermal conductivity of water at room temperature and pressure. For the range of temperatures and pressures stated above, one obtains a Prandtl number to the order of 10^{-2}. Consequently, the Peclet number varies from a small to a very large value, –being the product of ${\rm Re}$ and ${\rm Pr}$. As the injection Reynolds number is varied from 10 to 10^6, the Peclet number changes from 10^{-1} to 10^4. In this paper, we shall first consider the case of small Peclet numbers that corresponds to the lower end of the injection range.

In addition to the reciprocal of the Reynolds number that can always be used as a small perturbation

quantity, the problem exhibits an even smaller parameter that can be used in the asymptotic work. Using average values of $V \approx 5\,\text{m/s}$, $T_s \approx 3500\,\text{K}$, $T_w \approx 700\,\text{K}$, and $c_p \approx 1500\,\text{J/kg-K}$, it can be seen that the Eckert number in Eq. (7) is of the order of 6×10^{-6}. Being a measure of kinetic per sensitive energy, a small Eckert number is reflective of the dominant role of thermal energy compared with mean kinetic energy. This result is generally true inside a solid rocket motor except for a small region near the nozzle throat. The assumption of Ec being very small enables us to uncouple the energy equation from the momentum equation. As evident from Eq. (6), both velocity and pressure become very weak functions of temperature. We conclude that, whereas the temperature distribution is dependent on the velocity field, the converse is not true. This important realization justifies the decoupling of thermal effects, pioneered by Culick,[25] Flandro,[26] and co-workers, when analyzing the bulk gas motion in solid rocket motors.

E. Geometric Similarity Parameter

In the interest of algebraic clarity, the current analysis is carried out for $\phi^2 = 1$. This assumption will facilitate the algebraic effort and typifies aspect ratios used in upper stage rocket motors. Although these motors can sometimes exhibit spherical grains, a cylindrical grain is used in our analysis. A similar analysis using spherical coordinates is also possible. The use of a sensibly fictitious motor is important for the sake of simplicity. We expect the same approach to be repeatable for $\phi^2 \ll 1$. Evidently, as ϕ is modified, the solution is expected to change slowly. The $\phi^2 = 1$ case can thus capture the bulk features on a qualitative level.

III. Small Peclet Number Solution

While the Eckert number remains the smallest perturbation quantity in Eq. (6), the Peclet number can be used either as a small, or a large perturbation parameter depending on the size of Re. In rocket motors, the large Pe and large injection combination is the more likely scenario. In this section, however, the small Peclet, moderate injection case will be considered first. This academic solution applies for $\text{Re} \sim [10-100]$ and paves the way for the more elaborate treatment demanded by the large Pe case.

A. Double Perturbation Expansions

Forthwith, one can multiply Eq. (6) by Pe and expand each variable in the two perturbation parameters, $1/\text{Re}$ and Pe. Next, terms of zeroth order in both perturbation parameters can be collected. One obtains the energy equation at zeroth order,

$$\frac{1}{\eta}\frac{\partial}{\partial\eta}\left(\eta\frac{\partial T^{(0,0)}}{\partial\eta}\right)+\frac{\partial^2 T^{(0,0)}}{\partial z^2} = -\dot{Q} \tag{11}$$

where the first and second superscripts denote the order in $1/\text{Re}$ and Pe, respectively. Equation (11) is subject to the same boundary conditions given by Eq. (8).

Under the auspices of a small Pe, one can obviously study convective effects at the zeroth order in $(1/\text{Re})$ and the first order in Pe. In practice, one is able to evaluate the results by integrating nearly four hundred terms numerically. This is partly due to the failure of most symbolic packages in evaluating the resulting equations in a closed form. Since the scope of this study is to obtain a tangible formulation, we shall focus on the zeroth order solution in both $(1/\text{Re})$ and Pe. Using the same steps outlined in the leading-order solution, the asymptotic analysis developed here may be later repeated to obtain a higher-order approximation.

On inspecting Eq. (11), it can be concluded that the equation is linear and amenable to separation of variables. Using the method of superposition, a solution can be produced that is expressible in terms of eigenfunction expansions. Subsequent work is standard treatment for partial differential equations,[27] especially those encountered in heat transfer theory and applications.[28]

B. Eigenfunction Expansions

Using the concept of superposition, one can define

$$T^{(0,0)} = T_1^{(0,0)} + T_2^{(0,0)} + T_3^{(0,0)} \tag{12}$$

Due to the linearity of Eq. (11), one obtains a combination of two Laplace equations (with one nonhomogenous boundary condition) and one Poisson equation (with homogenous boundary conditions). These are

$$\frac{1}{\eta}\frac{\partial}{\partial\eta}\left(\eta\frac{\partial T_1^{(0,0)}}{\partial\eta}\right)+\frac{\partial^2 T_1^{(0,0)}}{\partial z^2} = 0 \tag{13}$$

$$T_1^{(0,0)}(\eta,0) = 1;\; T_1^{(0,0)}(\eta,1) = 0 \tag{14}$$

$$T_1^{(0,0)}(1,z) = 0;\; \frac{\partial T_1^{(0,0)}(0,z)}{\partial\eta} = 0 \tag{15}$$

$$\frac{1}{\eta}\frac{\partial}{\partial\eta}\left(\eta\frac{\partial T_2^{(0,0)}}{\partial\eta}\right)+\frac{\partial^2 T_2^{(0,0)}}{\partial z^2} = 0 \tag{16}$$

$$T_2^{(0,0)}(1,z) = 0;\; \frac{\partial T_2^{(0,0)}(0,z)}{\partial\eta} = 0 \tag{17}$$

$$T_2^{(0,0)}(\eta,0) = 0;\; T_2^{(0,0)}(\eta,1) = \hat{T} \tag{18}$$

$$\frac{1}{\eta}\frac{\partial}{\partial\eta}\left(\eta\frac{\partial T_3^{(0,0)}}{\partial\eta}\right)+\frac{\partial^2 T_3^{(0,0)}}{\partial z^2}=-\dot{Q} \tag{19}$$

$$T_3^{(0,0)}(1,z)=0;\ \frac{\partial T_3^{(0,0)}(0,z)}{\partial\eta}=0 \tag{20}$$

$$T_3^{(0,0)}(\eta,0)=0;\ T_3^{(0,0)}(\eta,1)=0 \tag{21}$$

C. Adding the Heat Source

So far, we have only been concerned with the simplifications affecting the energy equation. The reaction energy released inside a combustion chamber is another ingredient that needs to be appropriated. A heat source that closely mimics the energy released by propellant combustion is clearly necessary. Since chemistry is not taken into consideration here, the mass diffusion is ruled out. This leaves us with the option of distributing the thermal energy release in the same manner it is accounted for in basic two-dimensional models of premixed laminar flames. In that vein, the heat is produced in a thin sheet above the propellant surface. The corresponding thin-sheet approximation is conveniently modeled using the Dirac delta function (see Fig. 1 for the tentative positioning of the heat source). Mathematically, this may be expressed by

$$\dot{Q}=\dot{q}(z)\delta(\eta-b) \tag{22}$$

where $\dot{q}(z)$ is the rate of heat generation that may be allowed to vary along the chamber axis. The Dirac delta function and its properties are clearly described in Barton.[29]

D. Leading-order Solution

Equations (13) and (16) can be solved separately using separation of variables and eigenfunction expansions. They are then superimposed using Eq. (12) to construct the total solution at zeroth order in both perturbation variables.

To start, let us separate the variables using

$$T_1^{(0,0)}(\eta,z)=\Phi(\eta)\Psi(z) \tag{23}$$

Substituting this into Eq. (13), one gets

$$\frac{1}{\Phi}\frac{\mathrm{d}^2\Phi}{\mathrm{d}\eta^2}+\frac{1}{\eta}\frac{1}{\Phi}\frac{\mathrm{d}\Phi}{\mathrm{d}\eta}+\frac{1}{\Psi}\frac{\mathrm{d}^2\Psi}{\mathrm{d}z^2}=0 \tag{24}$$

This must be subjected to

$$\frac{\mathrm{d}\Phi}{\mathrm{d}\eta}(0)=0,\ \Phi(1)=0,\ \Psi(1)=0,\ \Psi(0)=1 \tag{25}$$

While the first two terms in Eq. (24) are function of η only, the last term is a function of z. They can differ only by a constant, say λ^2. We hence write

$$\frac{1}{\Phi}\frac{\mathrm{d}^2\Phi}{\mathrm{d}\eta^2}+\frac{1}{\eta}\frac{1}{\Phi}\frac{\mathrm{d}\Phi}{\mathrm{d}\eta}=-\frac{1}{\Psi}\frac{\mathrm{d}^2\Psi}{\mathrm{d}z^2}=-\lambda^2 \tag{26}$$

The negative sign preceding the separation constant is due to the homogeneity in boundary being in the r direction. The negative sign is hence necessary to obtain the eigenfunctions that are consistent with the physical characteristics of the problem at hand. From Eq. (26) two separate equations with their respective boundary conditions can be written. These are

$$\eta^2\frac{\mathrm{d}^2\Phi}{\mathrm{d}\eta^2}+\eta\frac{\mathrm{d}\Phi}{\mathrm{d}\eta}+\lambda^2\eta^2\Phi=0 \tag{27}$$

$$\frac{\mathrm{d}\Phi}{\mathrm{d}\eta}(0)=0,\ \Phi(1)=0 \tag{28}$$

and

$$\frac{\mathrm{d}^2\Psi}{\mathrm{d}z^2}-\lambda^2\Psi=0 \tag{29}$$

$$\Psi(1)=0,\ \Psi(0)=1 \tag{30}$$

Evidently, Eq. (27) is of the Bessel type with order zero. The general solution to this involves

$$\Phi(\eta)=C_1\mathrm{J}_0(\lambda\eta)+C_2\mathrm{Y}_0(\lambda\eta) \tag{31}$$

The boundary condition at the core dictates that C_2 be zero, while the boundary condition at the walls yield the eigenvalues. Eigenvalues are those values of λ that cause the function $\mathrm{J}_0(\lambda)$ to vanish at the specified boundaries. Of course, there can be an infinite number of eigenfunctions that need to be linearly superimposed in order to obtain the final solution in the radial direction. Each has the form

$$\Phi_n(\eta)=C_{1n}\mathrm{J}_0(\lambda_n\eta) \tag{32}$$

From Eq. (29), it is clear that the solution can be expressed in terms of hyperbolic functions such that

$$\Psi_n(z)=C_3\cosh\lambda_n z+C_4\sinh\lambda_n z \tag{33}$$

On one hand, the boundary condition at $z=1$ eliminates one constant and gives

$$C_3=-C_4\frac{\sinh\lambda_n}{\cosh\lambda_n} \tag{34}$$

On the other hand, the boundary condition at $z=0$ can be used to determine the constants in both radial and axial directions. Rewriting the solution in the z-direction, one has

$$\Psi_n(z)=C_5\sinh\lambda_n(1-z) \tag{35}$$

Using the definition of Eq. (23) and superimposing all eigenfunctions, one obtains

$$T_1^{(0,0)}(\eta,z)=\sum_{n=1}^{\infty}K_n\sinh\lambda_n(1-z)\ \mathrm{J}_0(\lambda_n\eta) \tag{36}$$

The non-homogeneous boundary condition at $z=0$ can now be used to determine K_n using the orthogonality property. As such, K_n is determined via

$$K_n=\frac{1}{\sinh\lambda_n}\frac{\int_0^1\eta\mathrm{J}_0(\lambda_n\eta)\,\mathrm{d}\eta}{\int_0^1\eta\mathrm{J}_0{}^2(\lambda_n\eta)\,\mathrm{d}\eta} \tag{37}$$

This can be further evaluated to yield

$$K_n = \frac{2}{\lambda_n} \frac{1}{\mathrm{J}_1(\lambda_n \eta) \sinh \lambda_n} \tag{38}$$

Likewise, Eq. (16) can be solved to get

$$K_n = \frac{2}{\lambda_n} \frac{\hat{T}}{\mathrm{J}_1(\lambda_n \eta) \sinh \lambda_n} \tag{39}$$

Solutions of Eqs. (13) and (16) can be added to get the following:

$$T_1^{(0,0)} + T_2^{(0,0)} = \sum_{n=1}^{\infty} \frac{2\mathrm{J}_0(\lambda_n \eta)\left[\sinh \lambda_n (1-z) + \hat{T} \sinh \lambda_n z\right]}{\lambda_n \sinh \lambda_n \ \mathrm{J}_1(\lambda_n \eta)} \tag{40}$$

Having derived a partial solution, we now proceed to solve the remaining Eq. (19). In the process, we exploit the presence of homogeneous boundary conditions and a heat source. From the homogeneous boundary conditions, one uses separation of variables to determine the eigenfunctions and eigenvalues arising in the r and z directions. Thus, from inspection of boundary conditions or by using separation of variables, it can be seen that the solution must have the double eigenfunction expansion form, namely,

$$T_3^{(0,0)} = \sum_{n=1}^{\infty} \sum_{m=1}^{\infty} B_{mn} \sin m\pi z \ \mathrm{J}_0(\lambda_n \eta) \tag{41}$$

Expanding Eq. (22) and using the property of orthogonality of eigenfunctions, one can determine the double eigenfunction expansion coefficients. These are

$$\dot{q}(z)\delta(\eta - b) = \sum_{n=1}^{\infty} \sum_{m=1}^{\infty} A_{mn} \sin m\pi z \ \mathrm{J}_0(\lambda_n \eta) \tag{42}$$

$$A_{mn} = \frac{\int_0^1 \int_0^1 \dot{q}(z)\delta(\eta - b) \sin m\pi z \ \mathrm{J}_0(\lambda_n \eta) \ \eta \, \mathrm{d}\eta \mathrm{d}z}{\int_0^1 \int_0^1 \sin^2 m\pi z \ \mathrm{J}_0{}^2(\lambda_n \eta) \ \eta \, \mathrm{d}\eta \mathrm{d}z} \tag{43}$$

$$A_{mn} = \frac{4\mathrm{J}_0(\lambda_n b)}{\mathrm{J}_1{}^2(\lambda_n)} \int_0^1 \int_0^1 \dot{q}(z) \sin m\pi z \ \mathrm{d}z \tag{44}$$

By substituting Eq. (41) into the left-hand-side of Eq. (19), it is possible to determine the A_{mn} coefficients by relating Eq. (41) to the double expansion coefficients of Eq. (44). After some effort, one arrives at

$$B_{mn} = \frac{A_{mn}}{m^2 \pi^2 + \lambda_n{}^2} \tag{45}$$

This completes our basic leading-order solution in both perturbation parameters. We now have

$$T^{(0,0)} = \sum_{n=1}^{\infty} \frac{2\mathrm{J}_0(\lambda_n \eta)\left(\sinh \lambda_n (1-z) + \hat{T} \sinh \lambda_n z\right)}{\lambda_n \sinh \lambda_n \ \mathrm{J}_1(\lambda_n \eta)} + \sum_{n=1}^{\infty} \sum_{m=1}^{\infty} B_{mn} \sin m\pi z \ \mathrm{J}_0(\lambda_n \eta) \tag{46}$$

At the next approximation level, convective heat transfer effects at zeroth order in $(1/\mathrm{Re})$ and first order in Pe can be captured. Convective effects appear to be unimportant here because of the large thermal energy and the correspondingly small injection-driven flow effect. Using the same perturbative treatment, the higher-order equation that results from retaining temperature terms to the first order in Pe can be gathered into

$$\frac{1}{\eta} \frac{\partial}{\partial \eta}\left(\eta \frac{\partial T^{(0,1)}}{\partial \eta}\right) + \frac{\partial^2 T^{(0,1)}}{\partial z^2} = u_r \frac{\partial T^{(0,0)}}{\partial \eta} + u_z \frac{\partial T^{(0,0)}}{\partial z} \tag{47}$$

where $u_r = -(1/\eta) \sin \frac{1}{2}\pi\eta^2$ and $u_z = \pi z \cos \frac{1}{2}\pi\eta^2$ are basic representations of the mean.[25,30] Here, the boundary conditions are homogeneous on all boundaries as was the case with solving Eq. (19). As such, the resulting set is amenable, in principle, to a solution using double eigenfunction expansions. Our experience shows, nonetheless, that in order to insure convergence, we need to consider at least the first 25 eigenfunctions in each direction. So for Eq. (47), we would have a minimum of 450 terms to integrate before realizing a sufficiently accurate solution. Since symbolic packages have failed so far to integrate the terms on the right-hand-side of Eq. (47), numerical integration was resorted to. In future work, we look forward to achieving more progress in this direction.

IV. Results

To better understand the solution behavior, we have plotted the constant temperature contour maps derived from $T^{(0,0)}$. In order to mimic the flame displacement above the burning surface, the heat source has been distributed in a thin sheet located at a radial distance of $b = 0.9$. We have chosen a spatially uniform heat generation in accordance with the standard thin sheet approximation. This may be justifiable insofar as averaging of unsteady flame variations over time results in a constant flame profile. We have considered three separate cases characterized by three orders of magnitude variations in the heat generation rate.

A. Case 1: $b = 0.9$, $\hat{T} = 0.8$ and $\dot{q} = 2.5$

For a sufficiently low heat generation rate, we observe in Fig. 2a a linear temperature gradient that increases away from the wall. Since the maximum temperature occurs at the core, the solution with low heat input is not a suitable model of the flame zone. The reason here can be attributed to the heat generation term being of the same order as the diffusion term. Note that the temperature variations along the boundaries are due to the asymmetric boundary conditions. The small fluctuations in those temperatures are due to the finite number of eigenvalues used in our code. In this study, we have used only 25 eigenvalues in the radial and axial directions. By carrying out a sensitivity analysis, we have found that further increase in the number of

eigenvalues (e.g., to 30) does not affect the solution in the interior. The small temperature variations along the boundaries, however, must be tolerated. It can be verified that the average value of these fluctuations over the radial and longitudinal lengths does essentially amount to the prescribed boundary condition. The justification for $\hat{T} = 0.8$ is derived from Eq. (9). Since our analysis has indicated that the values of $\hat{T}$ vary between 0.77 and 0.8, the upper limit has been chosen for convenience. The skewness observed in the temperature contours as we move in the downstream direction can be attributed to the relatively weak heat source. The slow variation in the temperature near the surface leads to a shallow temperature gradient that does not conform to temperature predictions in rocket motors. We conclude that the rate of heat release is not sufficient to reproduce the desired thermal field.

B. Case 2: $b = 0.9$, $\hat{T} = 0.8$ and $\dot{q} = 25$

In order to better simulate rocket motor conditions, the heat source is first increased by one order of magnitude. As shown in Fig. 2b, it can be seen that, for a large heat generation rate, a steeper gradient in temperature is obtained that can mimic the temperature gradient between the burning surface and the flame inside a solid rocket motor. Clearly, the nearly symmetric temperature map is the outcome of a dominant heat source and a weak convective motion. Also, the intense heat generation near $\eta = 0.9$ roughly approximates the mechanism of heat generation associated with a laminar premixed flame. However, by comparing the magnitude of the normalized temperature distribution to that obtained in a solid rocket motor, we realize that the observed distribution overestimates the maximum temperature in an actual motor. Since our normalized peak temperature of 2.2 corresponds to about 5000 K, it constitutes a modest exaggeration of practical values. In rockets, one would expect this temperature to fall in the vicinity of 3500 K. Since the imposed heat distribution rate is not derived from experimental data, it can be adjusted in a manner to produce realistic temperature maps. We thus conclude that a more appropriate value for heat generation should be used, namely, one that is closer to 12. When such a level is imposed, the thermal maps become a more adequate representation of the temperature field in a motor. This case is illustrated in Fig. 2c. Therein, the weak temperature variation in the axial direction can be attributed to the weak injection-driven flow effect in relative proportions with the thermal heat flow. The rapid temperature variation near the wall is also consistent with the steep thermal gradients observed in rockets. In fact, our analytical results appear to be in qualitative agreement with the numerical findings of Roh, Apte and Yang.[31]

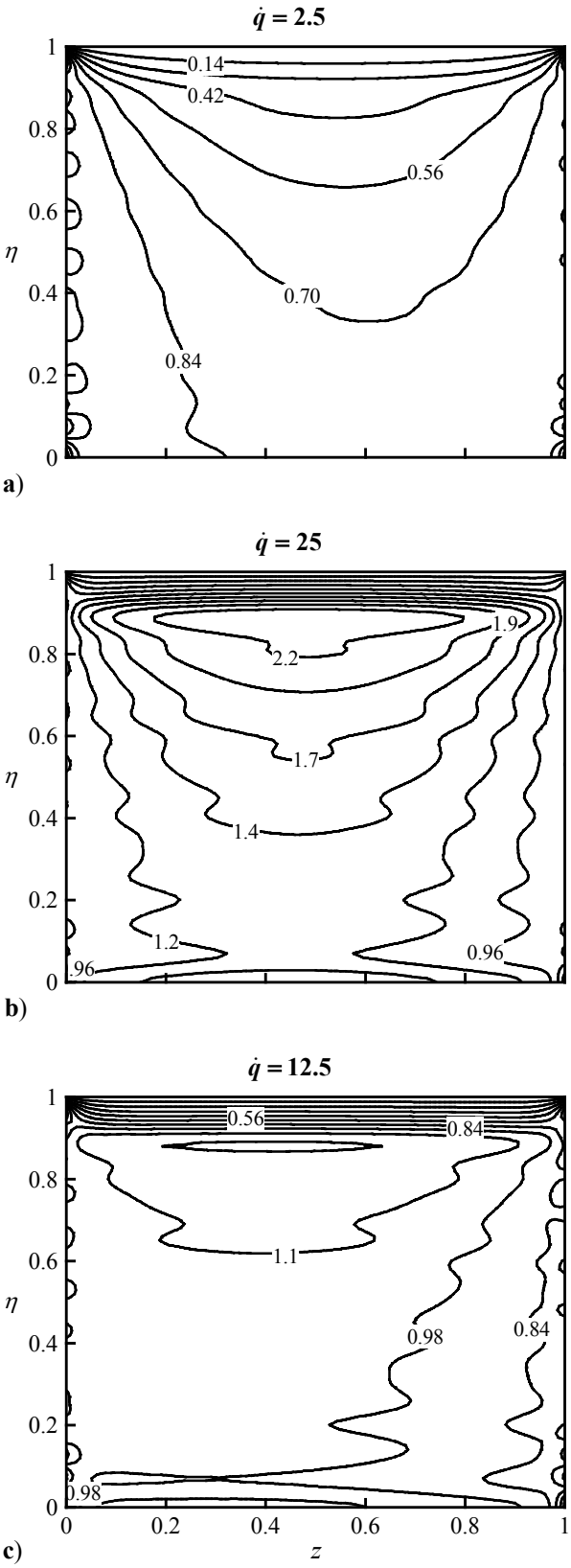

Fig. 2. Temperature contours for $b = 0.9$, $\hat{T} = 0.8$ and a) $\dot{q} = 2.5$, b) $\dot{q} = 25$, and c) $\dot{q} = 12.5$.

V. Conclusions

A preliminary investigation has been carried out to estimate the transport properties and physical quantities arising in the energy equation applied to a solid rocket motor chamber. The study reveals the presence of three contributing parameters. In ascending order, these are the Eckert number, the injection Reynolds number, and the Peclet number. The Eckert number is found to be so small that it leads to the uncoupling of temperature effects on the mean flow motion. This confirms the classic assumptions used by previous investigators. In the current study, the small Peclet, moderate injection case is considered. In later studies, the large Peclet, large injection case will be addressed. Our simplified analytical solution seems to crudely approximate the flame behavior and accompanying temperature maps. In the process, the usage of the Dirac delta function to effectuate the desired heat source displacement appears to be a viable artifact. The adequate agreement with temperature maps in rocket motors is reassuring. With further refinements, the asymptotic approach presented here appears to be worthy of consideration. For example, the analysis can be extended to a higher order by fully incorporating the convective mean flow effects. It can also be applied to spherical or rectangular motor chambers. The heat source location can be refined by relating b to the flame zone dynamics. In principle, the same approach outlined here can be applied to arrive at the large injection, large Peclet number solution. One of the obstacles that we anticipate stands in integrating the convective terms that can be very time consuming. To that end, better computer resources are needed to reach a solution in a reasonable amount of time. Also, use of symmetry methods and special functions need to be further explored for the possibility of providing other forms of analytical solutions.

References

[1]Culick, F. E. C., "Combustion Instabilities: Mating Dance of Chemical, Combustion, and Combustor Dynamics," AIAA Paper 2000-3178, July, 2000.

[2]Brewster, M. Q., "Solid Propellant Combustion Response: Quasi-Steady (Qshod) Theory Development and Validation," *Solid Propellant Chemistry, Combustion, and Motor Interior Ballistics*, Vol. 185, edited by V. Yang, T. B. Brill, and W.-Z. Ren, AIAA Progress in Astronautics and Aeronautics, Washington, DC, 2000, pp. 607-637.

[3]T'ien, J. S., "Oscillatory Burning of Solid Propellants Including Gas Phase Time Lag," *Combustion Science & Technology,* Vol. 5, 1972, pp. 47-54.

[4]De Luca, L. T., "Theory of Nonsteady Burning and Combustion Stability of Solid Propellants by Flame Models," *Nonsteady Burning and Combustion Stability of Solid Propellants*, Vol. 143, edited by L. T. De Luca, E. W. Price, and M. Summerfield, AIAA Progress in Astronautics and Aeronautics, Washington, DC, 1992, pp. 519-600.

[5]Margolis, S. B., and Williams, F. A., "Structure and Stability of Deflagrations in Porous Energetic Materials," *Solid Propellant Chemistry, Combustion, and Motor Interior Ballistics*, Vol. 185, edited by V. Yang, T. B. Brill, and W.-Z. Ren, AIAA Progress in Aeronautics and Astronautics, Washington, DC, 2000, pp. 549-590.

[6]Zemin, A. A., and Finjakov, S. V., "Burning Rate Response Functions of Composite-Modified Double-Base Propellants and Hmx," *Solid Propellant Chemistry, Combustion, and Motor Interior Ballistics*, Vol. 185, edited by T. B. B. a. W.-Z. R. V. Yang, AIAA Progress in Astronautics and Aeronautics, 2000, pp. 639-662.

[7]Beddini, R. A., and Roberts, T. A., "Response of Propellant Combustion to a Turbulent Acoustic Boundary Layer," *Journal of Propulsion and Power,* Vol. 8, No. 2, 1992, pp. 290-296.

[8]Flandro, G. A., "Effects of Vorticity on Rocket Combustion Stability," *Journal of Propulsion and Power,* Vol. 11, No. 4, 1995, pp. 607-625.

[9]Majdalani, J., and Roh, T. S., "Vorticity Dynamics in Isobarically Closed Porous Channels. Part 2: Space-Reductive Perturbations," *Journal of Propulsion and Power,* Vol. 17, No. 2, 2001, pp. 363-370.

[10]Culick, F. E. C., and Yang, V., "Prediction of the Stability of Unsteady Motions in Solid Propellant Rocket Motors," *Nonsteady Burning and Combustion Stability of Solid Propellants*, Vol. 143, edited by L. De Luca, E. W. Price, and M. Summerfield, Progress in Astronautics and Aeronautics, Washington, DC, 1992, pp. 719-779.

[11]Beddini, R. A., and Roberts, T. A., "Turbularization of an Acoustic Boundary Layer on a Transpiring Surface," *AIAA Journal,* Vol. 26, No. 8, 1988, pp. 917-923.

[12]Kirkköprü, K., Kassoy, D. R., and Zhao, Q., "Unsteady Vorticity Generation and Evolution in a Model of a Solid Rocket Motor," *Journal of Propulsion and Power,* Vol. 12, No. 4, 1996, pp. 646-654.

[13]Apte, S., and Yang, V., "Effects of Acoustic Oscillations on Turbulent Flowfield in a Porous Chamber with Surface Transpiration," AIAA Paper 98-3219, July, 1998.

[14]Vuillot, F., "Vortex-Shedding Phenomena in Solid Rocket Motors," *Journal of Propulsion and Power,* Vol. 11, No. 4, 1995, pp. 626-639.

[15]Apte, S., and Yang, V., "Effect of Acoustic Oscillation on Flow Development in a Simulated Nozzleless Rocket Motor," *Solid Propellant Chemistry,*

Combustion, and Motor Interior Ballistics, Vol. 185, edited by V. Yang, T. B. Brill, and W.-Z. Ren, AIAA Progress in Astronautics and Aeronautics, Washington, DC, 2000, pp. 791-822.

[16]Roh, T. S., Tseng, I. S., and Yang, V., "Effects of Acoustic Oscillations on Flame Dynamics of Homogeneous Propellants in Rocket Motors," *Journal of Propulsion and Power,* Vol. 11, No. 4, 1995, pp. 640-650.

[17]Roh, T. S., and Culick, F. E. C., "Transient Combustion Response of Homogeneous Propellants to Acoustic Oscillations in Axisymmetric Rocket Motors," AIAA Paper 97-3325, July, 1995.

[18]Vuillot, F., and Lupoglazoff, N., "Combustion and Turbulent Flow Effects in 2d Unsteady Navier-Stokes Simulations of Oscillatory Rocket Motors," AIAA Paper 96-0884, January, 1996.

[19]Vuillot, F., Dupays, J., Lupoglazoff, N., Basset, T., and Daniel, E., "2d Navier-Stokes Stability Computations for Solid Rocket Motors: Rotational, Combustion and Two-Phase Flow Effects," AIAA Paper 97-3326, July, 1997.

[20]Majdalani, J., Vyas, A. B., and Flandro, G. A., "Higher Mean-Flow Approximation for a Solid Rocket Motor with Radially Regressing Walls," AIAA Paper 2001-3870, July, 2001.

[21]Reid, R. C., Prausnitz, J. M., and Poling, B. E., *The Properties of Gases and Liquids*, 4th ed., McGraw Hill, New York, 1987, p. 388–490.

[22]Lucas, K., *Phase Equilibria and Fluid Properties in the Chemical Industry*, Dechema, Frankfurt, 1980.

[23]Lengelle, G., Duterque, J. and Trubert, J. F., "Physico-Chemical Mechanisms of Solid Propellant Combustion," *Solid Propellant Chemistry, Combustion, and Motor Interior Ballistics*, Vol. 185, edited by V. Yang, Brill, T. B., and Ren, W-Z, AIAA Progress in Astronautics and Aeronautics, 2000, pp. 287-334.

[24]White, F. M., *Fluid Mechanics*, 4th ed., McGraw Hill, 1999, p. 27.

[25]Culick, F. E. C., "Rotational Axisymmetric Mean Flow and Damping of Acoustic Waves in a Solid Propellant Rocket," *AIAA Journal,* Vol. 4, No. 8, 1966, pp. 1462-1464.

[26]Flandro, G. A., "Solid Propellant Acoustic Admittance Corrections," *Journal of Sound and Vibration,* Vol. 36, No. 3, 1974, pp. 297-312.

[27]Haberman, R., *Elementary Applied Partial Differential Equations with Fourier Series and Boundary Value Problems*, 3rd ed., Prentice-Hall, 1998.

[28]Kakac, S., and Yener, Y., *Heat Conduction*, Third ed., Taylor and Francis, 1993.

[29]Barton, G., *Elements of Green's Functions and Propogation*, Clarendon Press, Oxford, UK, 1989.

[30]Taylor, G. I., "Fluid Flow in Regions Bounded by Porous Surfaces," *Proceedings of the Royal Society, London, Series A,* Vol. 234, No. 1199, 1956, pp. 456-475.

[31]Roh, T. S., Apte, S., and Yang, V., "Combustion Dynamics of Homogeneous Solid Propellants in a Rocket Motor with Acoustic Excitations," *Solid Propellant Chemistry, Combustion, and Motor Interior Ballistics*, Vol. 185, edited by V. Yang, T. B. Brill, and W.-Z. Ren, AIAA Progress in Astronautics and Aeronautics, Washington, DC, 2000, pp. 885-906.